Cardiovascular Engineering and Technology, Vol. 10, No. 2, June 2019 *(© 2019)* pp. 380–393
https://doi.org/10.1007/s13239-019-00402-9

A Tunable Resonance Cantilever for Cardiac Energy Harvesting

THOMAS W. SECORD and MILAD C. AUDI

University of St. Thomas, St. Paul, MN 55105, USA

(Received 20 June 2018; accepted 22 January 2019; published online 1 February 2019)

Associate Editors Ajit P. Yoganathan and Scott C. Corbett oversaw the review of this article.

Abstract
Purpose—Energy harvesting from cardiac motion is an attractive means to avoid the use of batteries in implantable sensors and pacemakers. A single implantable device would ideally integrate both sensing and self-powering functionality. *Methods*—This work describes a novel electromagnetic system that achieves high sensitivity detection of the heart rate while simultaneously providing adaptive energy harvesting capability using a tunable resonance cantilever mechanism.
Results—Our prototype design exhibits tunability of resonant frequency across the range of physiologic heart rates at a combination of lengths and angular orientations. Our initial prototype also produces between 3.0 μW and 20.6 μW of power at heart rates of 79–243 bpm, respectively. *Conclusions*—The prototype device can harvest sufficient energy to sustain implantable cardiac devices such as a leadless pacemaker. The system in this paper has the potential to eliminate batteries in certain implantable cardiac devices and thereby improve overall patient monitoring and treatment.

Keywords—Energy harvesting, Resonance, Cardiology, Electromagnetic induction, Implantable medical devices, Pacemakers.

INTRODUCTION

Implantable devices that operate inside or near the heart have direct access to an immense collection of physiologic signals and therapy delivery methods. Classical cardiac devices such as pacemakers and implantable cardioverter defibrillators (ICDs) measure fundamental diagnostic signals including electrocardiogram (ECG), heart rate, respiration rate, and thoracic impedance. However, these devices require additional power budget to provide their wide functionality, and their continual energy expenditure for therapy delivery necessitates regular device explant and replacement. Therefore, efficient energy harvesting from the mechanical energy in cardiac motion is a highly desirable design feature that could eliminate the need for batteries in both sensing and therapy delivery devices.

Both the anatomical placement and design architecture fundamentally dictate the success of a device intended to capture energy from heart motion. Figure 1 shows an example of endocardial placement of our device near the right ventricular apex that would provide access to useful cardiac signals while also being ideally placed for direct integration into a right ventricular leadless pacemaker. In addition to proper placement, an energy harvesting device should be designed to match the frequency content of heart motion, which is particularly challenging given an excess of 200% variation in heart rate. The design discussed in this paper utilizes tunable resonance to achieve this goal.

Several researchers have explored power generation for biomedical devices and a summary is provided in Romero *et al.*[21] Most vibrational energy harvesters for biomedical applications obtain energy from motion of the extremities. In addition to being distant for cardiac applications, limb motion is completely absent during many hours of the day and during sleep. Therefore, cardiac motion, blood flow, arterial deformation, and arterial pressure fluctuations hold the best promise of continuous energy harvesting over a well-defined and predictable frequency range.

More generally, several devices have been explored for energy harvesting at all regions of the frequency spectrum and from a variety of energy input sources. A useful summary is provided by Khalig *et al.*[11] Within this broad range of research, electromagnetic systems (such as the device we propose) have been explored. For example, von Büren and Tröster[27] describe a device that uses a magnetic generator, yet it uses a flex-

Address correspondence to Thomas W. Secord, University of St. Thomas, St. Paul, MN 55105, USA. Electronic mail: thomas.secord@stthomas.edu, audi0003@stthomas.edu

ural suspension and exhibits a single, fixed resonant frequency that is higher than what would be required for cardiac applications. Perhaps most prominent in the literature are the numerous piezoelectric devices that have been studied extensively as a method for harvesting energy. Sodano *et al.*[24] provide an overview of many existing designs where resonance is a key operating requirement for optimizing the power output of a harvesting device. However, harvesting energy across a band of frequencies, such as the frequency range of heart rate, requires either a nonlinear mechanism (e.g., as in Ref. 12) or a resonant frequency that can be adjusted to match the excitation frequency.

Far fewer energy harvesting designs exist that utilize tunable resonance, yet some approaches have been proposed. For example, Challa *et al.*[2] and Hoffman *et al.*[7] utilize a magnetically imposed stiffness to tune the resonant frequencies of a harvesting system while a similar effect has been achieved using a compressive axial preload on a vibrating piezoelectric bimorph.[14] For cantilever-based harvesting systems, such as the one proposed in this paper, length adjustment has been explored as a means to tune resonant frequency. For example, Ref. 15 describes an automatic tuning mechanism for rotational motion and[4] describes a patented length adjustment system. Wu *et al.*[29] propose the use of mass position as an alternative mechanical method to adjust the resonant frequency of a cantilever-based system. Purely electrical methods for achieving tunable resonance have also been explored.[28] Other novel methods use simple ON-OFF tuning of discrete units within a vibrating strand.[22] None of these methods, however, are particularly well suited to cardiac applications that require miniaturization, encapsulation, and excitation at the relatively low mechanical frequencies of the heart rate.

Pfenniger *et al.*[18] provide a comprehensive summary of the most prominent results in energy harvesting that are specific to cardiac motion. Piezoelectric,[10] electromagnetic,[30,31] and electrostatic[25] approaches have all been explored for the purpose of cardiac energy harvesting. Notably, the nonlinear oscillator design by Karami and Inman[10] predicts a power output of 8 μW, while the imbalanced mass approach of Zurbuchen *et al.*[31] produced a power output of 17 μW. At these levels, conventional CMOS-based pacemakers could be readily powered. Some of the most complete *in vivo* results to date show a somewhat lower maximum power output of 1.7 μW.[30] A more hypothetical discussion of inertial energy harvesting from heart motion is provided by Deterre *et al.*[3] and other, motion-independent, methods have also been employed for energy harvesting to power cardiac devices.[5] All of the foregoing cardiac energy harvesting devices are similar in that they have fixed dynamic behavior: a fixed resonant frequency, a fixed nonlinear vibration, or a fixed mechanical assembly.

Our present work is unique within the literature given its integration of heart rate sensing and its use of both gravitational orientation and cantilever length adjustment as a means to adaptively harvest energy at the relatively low frequencies of the heart rate. Our tuning mechanism is also geometrically suited to catheter placement. With this novel functionality and geometry, the resonant frequency of our device can be periodically adjusted to match the heart rate, thereby providing maximum power output across the physiologic range of heart rates. Our present work significantly extends our previous work in Ref. 23 through a new resonance tuning mechanism, additional theoretical analysis, and enhanced experimentation.

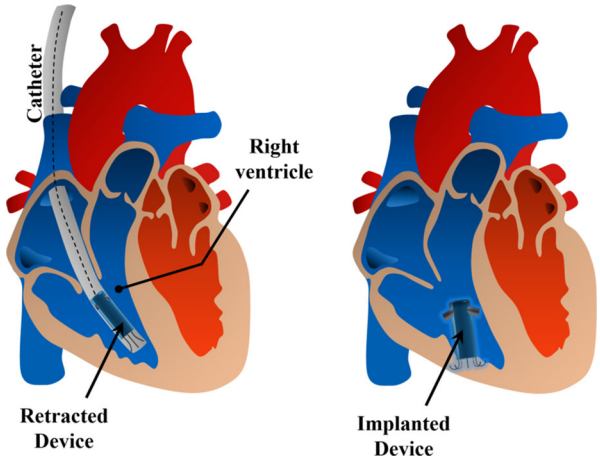

FIGURE 1. Example implant method and site for a dual sensing and energy harvesting device.

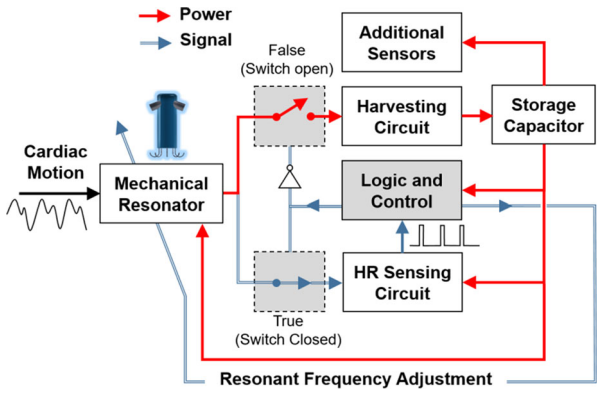

FIGURE 2. Schematic representation of the adaptive energy harvesting system shown in its resonance tuning mode.

MATERIALS AND METHODS

Design Architecture and Power Budget

The proposed system operates by periodically alternating between harvesting and resonance adaptation modes. Figure 2 shows a schematic representation of the system. The resonance adaptation mode is used to periodically measure heart rate (on the time scale of substantial heart rate variation) in order to adaptively tune the resonant frequency to match the heart rate and maintain maximum energy harvesting output over time. The process is supervised by a central control unit that switches between the harvesting and adaptation mode. With sufficient energy harvesting performance, additional sensors can be continuously logging data. Therefore, the device is best described as a dual harvesting and sensing system.

We model the flow of energy for a general tunable resonance energy harvesting system as shown in Fig. 3. The left portion of the figure shows the temporal logic states denoted by the boolean variables S_H, S_T, S_S, and S_L to define when the harvesting, resonance tuning, sensing, and logic modes are activated, respectively. A likely mode of operation relates these variables such that when the device is collecting energy it is also simultaneously powering on-board sensors. When the device is tuning its resonant frequency, however, both the sensing and harvesting functionality are turned off. On-board logic that governs the switching states must remain on continuously. Expressed in terms of the boolean variables, we will assume $S_H = \neg S_T$, $S_H = S_S$, and $S_L \equiv 1$ where $\neg$ denotes logical negation. The period of tuning, T_T, is assumed to be fixed and the actual tuning process occurs with a duty cycle of τ where $0 < \tau < 1$.

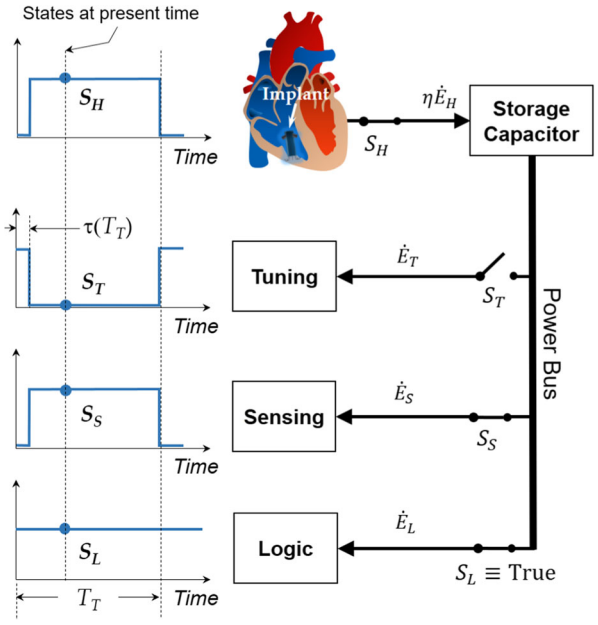

FIGURE 3. Energy flow and timing diagram for an actively tunable energy harvesting system.

We define the power input to the system through the harvesting mechanism as $\eta\dot{E}_H$ where $\dot{E}_H$ is the output of the harvesting coil and η is the efficiency of the associated harvesting circuitry. Similarly, $\dot{E}_T$, $\dot{E}_S$, and $\dot{E}_L$ represent the sunk power for tuning, sensing, and logic, respectively. Note that $\dot{E}_L$ also includes any quiescent power requirements of the device. With these definitions, maintaining a viable energy balance (i.e., an increase in the energy stored over time) requires that the following inequality is satisfied by the on-board logic:

$$\eta\dot{E}_H(1-\tau) \geq \tau\dot{E}_T + (1-\tau)\dot{E}_S + \dot{E}_L. \qquad (1)$$

The architecture in Fig. 2 and timing in Fig. 3 show the harvesting and resonance tuning modes as mutually exclusive. As a numerical example of power budgeting in this architecture, we will assume an average harvested power of approximately $\eta\dot{E}_H = 8\ \mu$W given that this value is within the range of feasible power values for the prototype device described in this work (see "Experimental Setup and Results" section). If we also assume the tuning mechanism power requirement is $\dot{E}_T \approx 100$ mW,[6] the allocated sensor power budget is $\dot{E}_S = 0.25\ \mu$W, and the continuous power dissipation budget (for logic and other quiescent supply) is $\dot{E}_L = 0.25\ \mu$W, then to maintain a viable energy balance, the maximum possible duty cycle for tuning (i.e., the maximum fraction of operating time the device is allowed to tune itself) is $\tau = 7.5 \times 10^{-5}$ as obtained from (1). If the tuning operation itself takes approximately 40 ms (assuming an actuator velocity of 5 mm/s and a typical tuning length of 0.2 mm), then the minimum allowable tuning period, T_T, is 8.9 min. Viewed in the context of results in "Results" section and presently available actuator technology as in Ref. 6, a power budget with these orders of magnitude is feasible and will allow for a device that can track sustained physiological changes in heart rate. Moreover, strategic variation of the tuning period (e.g., tuning only during active hours) would allow for significantly more frequent tuning.

Specific Design Concept

We explored the design concept space with three specific physical considerations in mind:

1. Low mechanical resonant frequencies require large mass, small stiffness, or both;

2. Tuning resonance requires modulation of mass, stiffness, or both; and
3. Physical motions that adjust resonant frequency should themselves require minimal energy and zero holding power.

Our original work in Ref. 23 produced resonant frequencies above the physiologic range of heart rates. Therefore, in this work, we have modified our approach to utilize a variable length cantilever to satisfy these three considerations at lower resonant frequencies. Figure 4 shows the cross sectional view of the specific device design concept. The salient features of the device concept include the oscillating magnet tip mass and an electromechanical beam length adjustment mechanism. The oscillating tip magnet travels into the pickup coils whose voltage will either be used in heart rate sensing or applied across an energy harvesting circuit. The generated coil voltage arises from Faraday's law, a principle which serves as an alternative to a rechargeable battery in some commercialized devices.[17]

We address the first of the three considerations (low resonant frequencies) through small stiffness behavior arising from the elastic deformation of a thin cantilever. For a cantilever of length L, its stiffness is strongly dependent upon its length (going as $\frac{1}{L^3}$), and, with sufficient elongation, can thereby provide the low required stiffness for a given moving magnet mass. We address the second consideration (tunable resonance) through the adjustable length mechanism shown in Figs. 4 and 5 and the use of gravitational orientation. We address the third and final design consideration (low power tuning) through the use of a linear piezoelectric motor (also shown in Figs. 4 and 5). Off-the-shelf technologies exist for this purpose that universally exhibit non-backdriveability and zero holding power.[6] These traits make piezoelectric linear motors ideally suited to low-energy, accurate cantilever length adjustments.

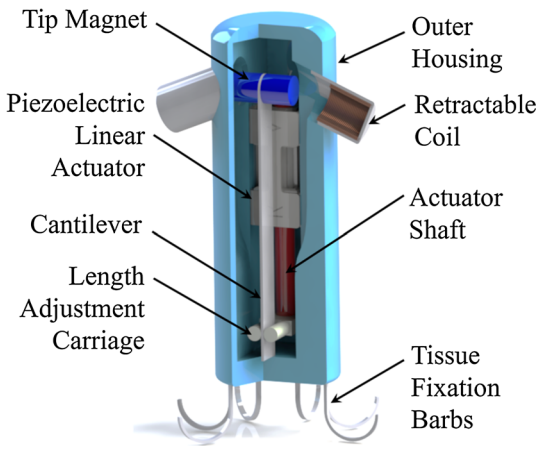

FIGURE 4. Cross sectional view showing the device design and associated components.

Design Operation

The two device configuration extremes are shown in Figs. 5a and 5b. Figure 5a shows the maximum length configuration. This provides the lowest effective stiffness and lowest resonant frequency. Figure 5b shows the minimum length configuration. At this extreme of operation, the system exhibits the highest effective stiffness and highest resonant frequency. Periodic tuning to operate between these extremes provides the opportunity for mechanical resonance across the entire range of physiologic heart rates as discussed in the next sub-section.

Heart Rate Variation Considerations

There are two primary time scales of interest in the design of a tunable resonance device for cardiac sensing and energy harvesting. The first time scale is the time scale of the heart rate itself (1–3 Hz) over which the device must provide high-quality (i.e., narrow band) mechanical resonance. Although some frequency content near 25 Hz exists in the heart chamber accelerations, prior analysis showed that available power at this frequency is nearly ten times lower than

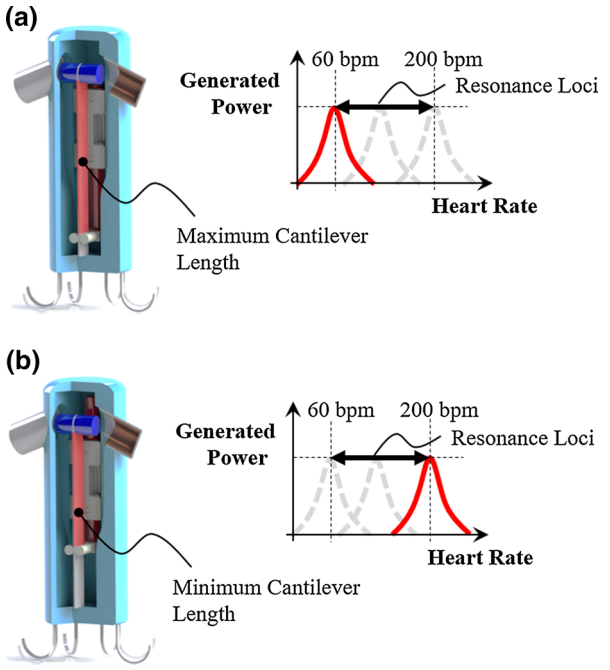

FIGURE 5. Device operation for (a) minimum resonant frequency and (b) maximum resonant frequency.

that in the frequency range of the heart rate.[3] The second time scale is the slower time scale of heart rate variation over which the device must adapt its resonant frequency to match the current heart rate. Together these time scales are crucial design inputs.

With regard to the slower time scales of heart rate variation, standard methods exist for quantifying spectral content in various frequency ranges.[1] The design goal for this work is to allow for heart rate tracking on the order of the ultra-low and very-low frequency ranges of 0.0033–0.04 Hz or, equivalently, periods ranging from 25 to 300 s. A device that could periodically tune its resonant frequency at these time scales, without undue energy expenditure, could provide sufficiently fast adaptation to heart rate variation in response to activity level, stress, and body temperature. Furthermore, the resonance modulation frequency itself can be logged by the device and used as a prognostic signal.[9]

Theoretical Model Development

One of the goals of this work is to establish a rigorous, analytically insightful, theoretical model for use in device design, scaling, and refinement. This section describes the dynamics of device operation using an Euler–Bernoulli and Rayleigh framework that captures the lowest natural frequency of the cantilever beam system. The dynamic model accounts for both the energy harvesting and heart rate sensing modes of operation. The model also encompasses the various possibilities for device orientation. Orientation of the device axis with respect to gravity is an important consideration for the device performance. The case of gravitational alignment and gravitational orthogonality are treated as separate, bounding cases for the dynamic model.

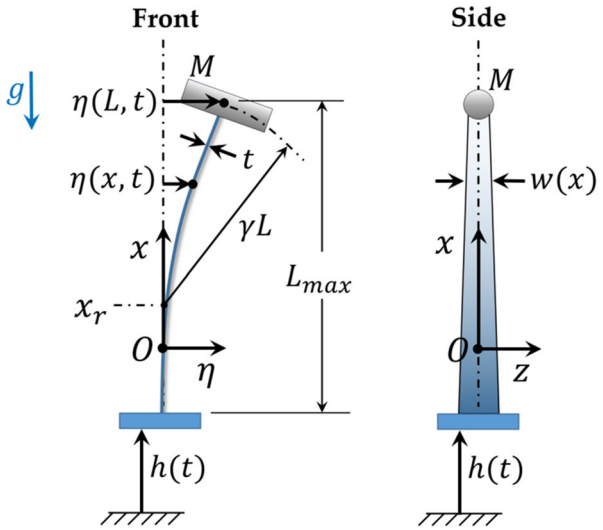

FIGURE 6. Cantilever beam kinematics and geometric definitions as viewed in the gravitationally aligned configuration.

Gravitationally Aligned Model

Figure 6 shows a beam of adjustable length L (measured from the origin O) with a tip mass M whose x-axis is parallel to the direction of gravity. The beam has a bending moment of inertia, $I(x)$, that is lowest about z-axis. Given this deliberate asymmetry in the flexural rigidity, the beam will maintain planar spatial kinematics in the lateral displacement variable $\eta(x, t)$ as shown in the front view in Fig. 6.

Our model includes the bending strain energy V_b, gravitational potential energy V_g, work done by the axial inertial forces V_a, and translational kinetic energy T. The supplied displacement from the heart wall, $h(t)$, is measured with respect to an inertial frame. This may be viewed as the heart wall displacement except in cases when the patient is undergoing true inertial accelerations of comparable magnitude to those imposed by the heart wall motion. In all but the trivial case of unperturbed orthogonality, the heart wall motion will supply energy to the lateral deflection modes of the cantilever. This energy channeling to lateral deflection is facilitated particularly well when periodic motions of the heart wall displacement are near the fundamental resonant frequency of the same stationary cantilever in the absence of such axial excitation. Our approach is based on this dynamic principle.

Following an approach similar to Lee,[13] the total kinetic energy, T, of the beam and tip mass is given by

$$T = \frac{1}{2} M \left[\left(\frac{\partial \eta(L,t)}{\partial t} \right)^2 + \dot{h}^2 \right] + \frac{1}{2} \int_0^L \lambda(x) \left[\left(\frac{\partial \eta(x,t)}{\partial t} \right)^2 + \dot{h}^2 \right] dx \tag{2}$$

where $\lambda(x)$ is the linear mass density of the beam. For a constant material density ρ, constant thickness t, and varying width $w(x)$, this can be written as $\lambda(x) = \rho t w(x)$.

In the gravitationally aligned cantilever, deflections of the tip mass will result in a non-negligible change in the gravitational potential energy. The vertical motion of the mass is approximated using the effective radius γL ($\gamma < 1$) shown in left portion of Fig. 6. Taking the tip angle with respect to vertical as $\theta = \frac{\partial \eta(L,t)}{\partial x}$, we obtain the following gravitational potential energy:

$$V_g = Mg\gamma L(\cos\theta - 1) \tag{3}$$

The bending strain energy expression is invariant under gravitational orientation and is given by

$$V_b = \frac{1}{2}\int_0^L EI(x)\left(\frac{\partial^2\eta(x,t)}{\partial x^2}\right)^2 dx \tag{4}$$

Finally, potential energy associated with axial inertial forces is also invariant under orientation and is given by

$$V_a = \frac{1}{2}\int_0^L \left[-\lambda(x)(L-x)\ddot{h} - M\ddot{h}\right]\left(\frac{\partial\eta(x,t)}{\partial x}\right)^2 dx \tag{5}$$

The electromagnetic transduction coil is assumed to be attached in series with a constant and matched resistance, R_h, during harvesting and attached to a high input impedance circuit when sensing. Therefore, the dynamics of energy harvesting require inclusion of this dissipative effect, while the dynamics of sensing do not. This will be reflected through the use of the Boolean variable S_H where

$$S_H = \begin{cases} 0 & \text{Harvesting inactive} \\ 1 & \text{Harvesting activated} \end{cases} \tag{6}$$

The electromagnetic coupling constant of the coil, K_v, arises from Faraday's law and is most reliably obtained experimentally. Although this constant would be expected to change with the position of the magnet within the coil, we will assume a mean value across the range of magnet motion for the purpose of model development.. The non-conservative force, F_{nc}, acting at the tip of the cantilever will be $K_v i$ where i is the current flowing through both the harvesting resistance, R_h, and the coil resistance, R_c. Because the motion of the magnet induces a voltage of $K_v\frac{\partial\eta(L,t)}{\partial t}$, the overall force can then be expressed as

$$F_{nc} = \frac{K_v^2}{R_c + R_h}\left(\frac{\partial\eta(L,t)}{\partial t}\right) \tag{7}$$

In preparation for the use of Rayleigh's method, we will assume a single mode oscillation prescribed by separable spatial and time functions: $\eta(x,t) = \phi(x)\psi(t)$. The Lagrangian for the system is $L = T - V_b - V_g - V_a$. To account for the non-conservative force imposed from the energy harvesting process, we define the Rayleigh dissipation function as

$$F = \frac{1}{2}\left(\frac{K_v^2\phi(L)^2}{R_c + R_h}\right)\dot{\psi}^2 \tag{8}$$

Prior to executing Lagrange's equation, $\frac{d}{dt}\left(\frac{\partial L}{\partial\dot{\psi}}\right) + \frac{\partial F}{\partial\dot{\psi}} - \frac{\partial L}{\partial\psi} = 0$, we recognize that practical designs will require a magnet mass that is significantly greater than the cantilever mass (i.e., $\int_0^L \lambda(x)dx << M$). Therefore, we neglect the contribution of the thin cantilever to the energy storage in the system. This assumption retains only the first term in (2) and the second integrand in (5). The resulting equation of motion for the gravitationally aligned configuration shown in Fig. 6 is then

$$M\phi(L)^2\ddot{\psi} + S_H\left(\frac{K_v^2\phi(L)^2}{R_c + R_h}\right)\dot{\psi} + \left[E\int_0^L I(x)(\phi'')^2 dx - M\ddot{h}\int_0^L(\phi')^2 dx - Mg\gamma L(\phi'(L))^2\right]\psi = 0 \tag{9}$$

where ϕ', ϕ'', $\dot{\psi}$, and $\ddot{\psi}$ denote first and second derivatives in position and time, respectively.

We invoke Rayleigh's method and assume that the mode shape $\phi(x)$ can be well approximated by the statically deflected shape of a tip loaded cantilever with a maximum tip deflection δ_{tip} (the exact value of which is inconsequential):

$$\phi(x) = \frac{\delta_{tip}}{2}\left(3\left(\frac{x}{L}\right)^2 - \left(\frac{x}{L}\right)^3\right) \tag{10}$$

Substitution of (10) into (9) and further assuming that $I(x)$ is constant along the beam length yields the following Mathieu-type differential equation:

$$M\ddot{\psi} + S_H\left(\frac{K_v^2}{R_c + R_h}\right)\dot{\psi} + \left[\frac{3EI}{L^3} - \ddot{h}\left(\frac{6M}{5L}\right) - \frac{9Mg\gamma}{4L}\right]\psi = 0 \tag{11}$$

The dynamics of sensor operation are identical to (11), yet with the dissipation term neglected since $S_H = 0$.

Stability Analysis of the Gravitationally Aligned Cantilever

The stability of the cantilever system is established by the sign of the rightmost bracketed term of (11). In this term, the beam tip stiffness is used to scale the remaining terms yielding the following dimensionless stiffness:

$$\bar{k} = 1 - \frac{2M\ddot{h}L^2}{5EI} - \frac{3Mg\gamma L^2}{4EI} \tag{12}$$

We now let $\gamma = \frac{L - x_r}{L}$ where x_r is the point along the x-axis treated as the center of rotation for the beam tip motion (see Fig. 6). This point is taken to reside at the intersection of the line tangent to the point $\eta(L,t)$ with the x-axis. For the assumed mode shape in (10), $\gamma = \frac{2}{3}$. The second term in (12) is often small in relation to unity whereas the third term can be of order unity. The ratio of the second and third terms in (12) yields $\frac{4}{5}\frac{\ddot{h}}{g}$, which will be small during the expected device usage.

Dropping the second term in (12) and using $\gamma = \frac{2}{3}$ yields a convenient stability criterion. Namely, the gravitationally aligned vibrational motion is stable when $\bar{k} > 0$, or

$$L < \sqrt{\frac{2EI}{Mg}} \tag{13}$$

This constraint on the length reflects the length beyond which $\frac{d^2}{d\phi^2}(V_g + V_b) < 0$ and the vertically oriented cantilever becomes an unstable equilibrium. For small perturbations of cantilever designs that exceed this length, the tip mass continues to fall downward by overcoming the ability of the bending stiffness to return the tip mass to its vertical equilibrium. This will be referred to as the cantilever droop failure mode. The droop failure mode is more restrictive than the buckling from tip mass, which occurs when $L > \frac{\pi}{2}\sqrt{\frac{EI}{Mg}}$.

Gravitationally Orthogonal Model

All gravitationally orthogonal orientations have the same governing differential equation because the gravitational potential energy derivative becomes zero in Lagrange's equation. Therefore, for the gravitationally orthogonal model, there is no dependence upon rotation about the beam's longitudinal axis provided that the axis itself is orthogonal to gravity. As described in the stability analysis above, the acceleration term in (12) is also small. Given these simplifications, the modified form of (11) for the gravitationally orthogonal configurations is

$$M\ddot{\psi} + S_H\left(\frac{K_v^2}{R_c + R_h}\right)\dot{\psi} + \left(\frac{3EI}{L^3}\right)\psi = 0 \tag{14}$$

Design for Cardiac Excitation

Equations (11) and (14) are the basis for useful design exploration in the space of resonant frequency as function of beam flexural rigidity and length. Both the scale of the system and the natural frequency must be well matched to the heart. In the gravitationally aligned case, the natural frequency, $f_{n,a}$ is extracted from (11):

$$f_{n,a} = \frac{1}{2\pi}\sqrt{\frac{3EI}{ML^3} - \frac{3g}{2L}} \tag{15}$$

In the case of orthogonal orientation with respect to gravity, the natural frequency is extracted from (14):

$$f_{n,o} = \frac{1}{2\pi}\sqrt{\frac{3EI}{ML^3}} \tag{16}$$

The natural frequency relationships in (15) and (16) are best explored graphically under realistic design constraints. Specifically, we consider the design scenario in which flexural rigidity of the cantilever, EI, and cantilever length, L, can be varied as the primary design parameters following selection of a desired magnet whose mass, M, is known. This approach most accurately captures the discrete nature of commercially available magnets and the continuous nature of the fabricated cantilever dimensions.

To illustrate the design procedure and provide a proof-of-principle prototype, we selected a readily available neodymium magnet mass M of 0.75 g. The corresponding design surfaces are shown in Figs. 7a and 7b for the gravitationally aligned and gravitationally orthogonal cases, respectively. The flexural rigidity range was chosen to represent typical polymeric cantilevers with sub-millimeter thickness and widths on the order of millimeters. Similarly, the

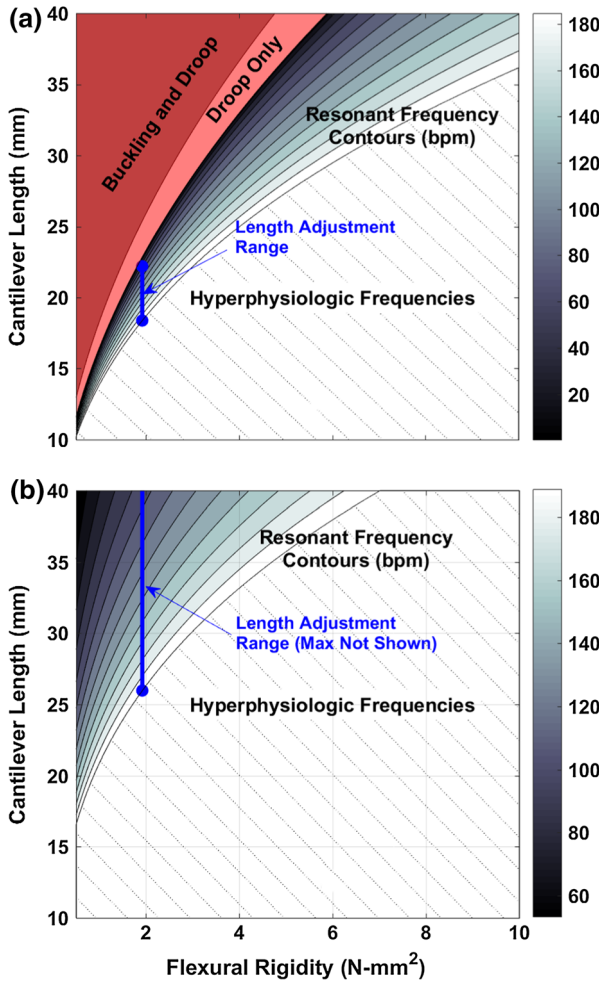

FIGURE 7. Cantilever design space for a tip mass of M = 0.75 g. (a) Gravitationally aligned natural frequency contours. (b) Gravitationally orthogonal natural frequency contours.

length scale was chosen to represent lengths on the order of tens of millimeters. These design scales allowed for fabrication of a proof-of-principle prototype as described in "Results" section.

Figure 7a highlights the required length adjustment range to achieve resonant frequencies in the physiologic heart rate range when the device is operating in a gravitationally aligned state. The lighter shaded contours represent high frequencies that require a shorter cantilever length while the darker shaded contours show the low frequencies achieved at longer cantilever lengths. Our prototype design uses a flexural rigidity of 1.9 N-mm^2, which requires the beam length to be adjusted between 18 and 23 mm to achieve resonant frequencies between 200 and 60 bpm, respectively. As the beam is elongated, the design approaches the droop failure mode, but the final design prevents cantilever droop from occurring in practice because the cantilever housing will maintain the cantilever in a predominantly upright position. The cantilever can then reinitiate oscillation following simple algorithmic length adjustment during operation.

Figure 7b presents the gravitationally orthogonal resonant frequency surface contours. As in Fig. 7a, the lighter shaded contours represent higher frequencies that require shorter cantilever length to achieve, while the darker shaded contours show the low frequencies achieved at longer cantilever lengths. In the initial prototype, the required beam length now must be varied between 26 and 60 mm in order to achieve physiologic resonant frequencies. In this case, the droop and buckling failure modes are no longer present. The selected flexural rigidity and tip mass are suitable for a design operating near 25 mm because the gravitationally orthogonal orientation is analyzed as a bounding case for device operation. If the device is implanted to remain as gravitationally aligned as possible during both upright and prone or supine postures, then physiological natural frequencies can be achieved with the adjustable cantilever mechanism.

Figure 7a illustrates that the resonant frequency contours compress significantly at smaller scales leading to minimal variation in length to achieve the desired frequency tuning range. This suggests that small scale devices could be designed around the gravitationally orthogonal case where sensitivity to length is considerably lower as evidenced by the broader and more vertical contours in Fig. 7b. Tuning resonant frequency over the physiologic range will be possible in the aligned case using shorter overall lengths yet will require a length adjustment mechanism with sufficient motion resolution and precision.

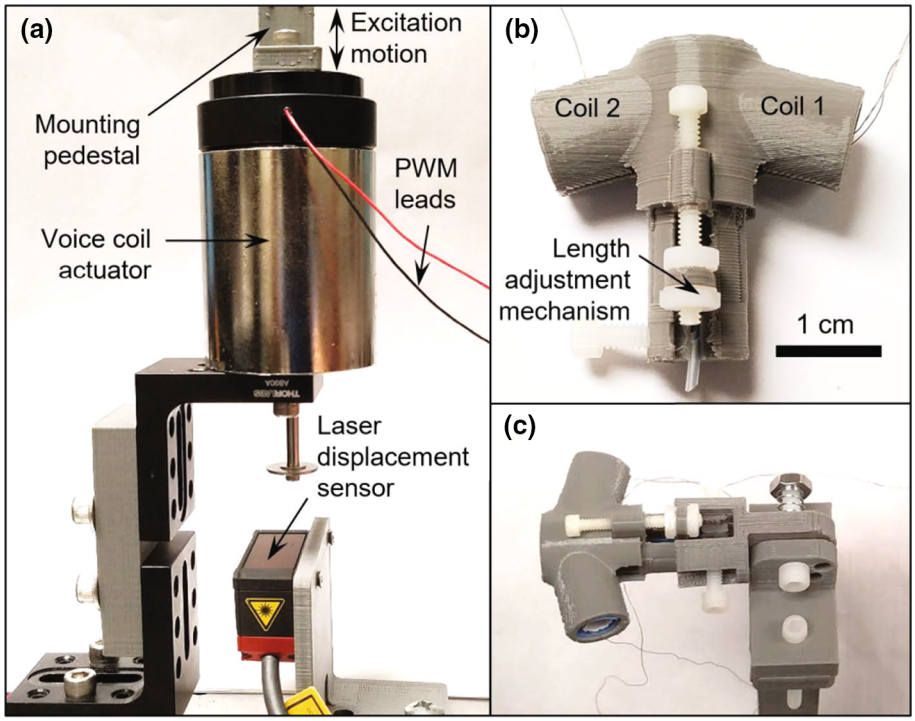

FIGURE 8. Prototype assembly and experimental apparatus for demonstrating tunable resonance energy harvesting performance in multiple gravitational orientations. (a) Construction of a closed-loop voice coil system capable of precisely controlling input excitation displacement. (b) Prototype construction using two coils and a manual length adjustment mechanism. (c) Prototype attached to the mounting pedestal and fixture.

RESULTS

Prototype Description

Our initial prototype was designed using the flexural rigidity and length dimensions provided in the theoretical modeling discussion of "Design for Cardiac Excitation" section. The prototype assembly is shown in Figs. 8b and 8c with the inner magnet and cantilever structure shown in Fig. 9c. The prototype allows for continuous length adjustment between 23 and 13 mm as controlled by a length adjustment carriage shown in the initial concept figures (Figs. 4 and 5). To maintain a focus on the tunable resonance concept, rather than hardware design, the prototype length adjustment mechanism uses a manual adjustment lead screw and a 3D printed housing. The cantilever is made from a polyester strip ($E \approx 4.2$ GPa) with a constant cross section (2.5 mm wide by 0.13 mm thick). The prototype is rigidly attached to a mounting plate undergoing axial excitation at an adjustable angle with respect to gravity. Additional details of the experimental setup are provided in "Experimental Setup and Results" section. To provide the spatially oscillating magnetic field, we symmetrically secured two neodymium magnets (3.2 mm diameter by 6.4 mm length) to the cantilever tip as shown in Fig. 9c. The combined mass of the magnets is 0.75 g. The prototype also contains two serially-connected coils, each having a length of 6.4 mm, a mean diameter of 7.6 mm, and 400 turns of 0.13 mm magnet wire. The resulting voltage gain of the coil and magnet combination is approximately 300 μV s mm^{-1} with each coil having an individual resistance of 13.8 Ω. The overall inner construction of the device reflects the layout shown in Fig. 4.

Using the dimensions and parameters described above, (15) predicts a gravitationally aligned resonant frequency of 0.5 Hz (30 bpm) using the achieved maximum length of 23 mm, while (16) predicts a gravitationally orthogonal resonant frequency of 4.1 Hz (246 bpm) at this length. By reducing the length by 1–22 mm, the new gravitationally aligned resonant frequency is predicted to be 1.2 Hz (69.1 bpm) and the new gravitationally orthogonal resonant frequency is predicted to be 4.3 Hz (257 bpm). We experimentally explored these length conditions at various gravitational orientations.

Experimental Setup and Results

We tested the energy harvesting prototype at three different gravitational angles (0°, 45°, 90°) as shown in Fig. 9. At each angle, the resonant frequency was established at a cantilever length of 22 and 23 mm. In the experimental setup shown in Fig. 8a, the prototype was placed onto a 24 cm pedestal extension in order to sufficiently isolate the harvesting coil and cantilever magnet from the magnetic field of the driving voice coil actuator. The voice coil was driven using a pulse width modulation (PWM) amplifier in a position control loop with a 4 mm peak-to-peak sinusoidal displacement command waveform and a feedback displacement signal from a Micro Epsilon ILD1420-25 laser displacement sensor. The excitation displacement is modest with respect to the motion of possible harvester placement sites discussed in Zurbuchen *et al.*[31] The frequency of the input waveform was swept continuously from 48 and 180 bpm (0.8–3 Hz) for the 0° and 45° conditions and was extended to span 48–300 bpm (0.8–5 Hz) for the 90° case given its higher resonant frequencies. The output of the harvesting coil was applied across a harvesting resistance of $R_h = 27.6$ Ω (matched to the series connection of the two coils). The voltage of the resulting output across the harvesting resistance was amplified and filtered in analog circuitry, and then sampled using a National Instruments PCIe-6343 data acquisition board. The measured voltage across the harvesting resistance, $V_{out}(t)$, was then converted to instantaneous power as $V_{out}(t)^2/R_h$.

Performance data for the harvester are shown in Fig. 10 for the three different gravitational angles. Within each angle condition, we tested for resonant frequency change using a 1 mm length reduction from the maximum length of 23 mm. In all cases, we used a 4

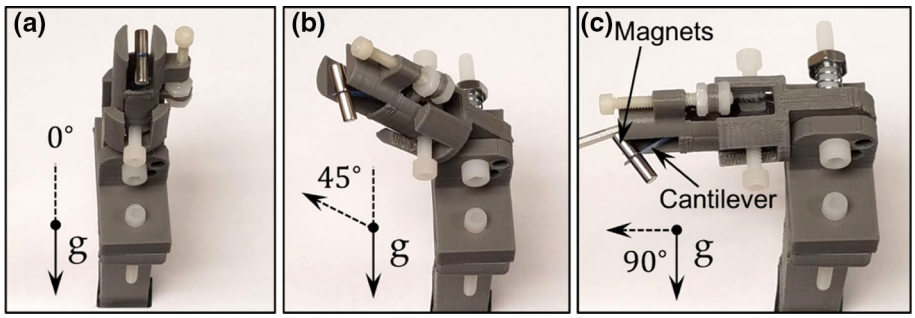

FIGURE 9. Prototype mechanism shown at the three tested angles (a) 0°, (b) 45°, and (c) 90°.

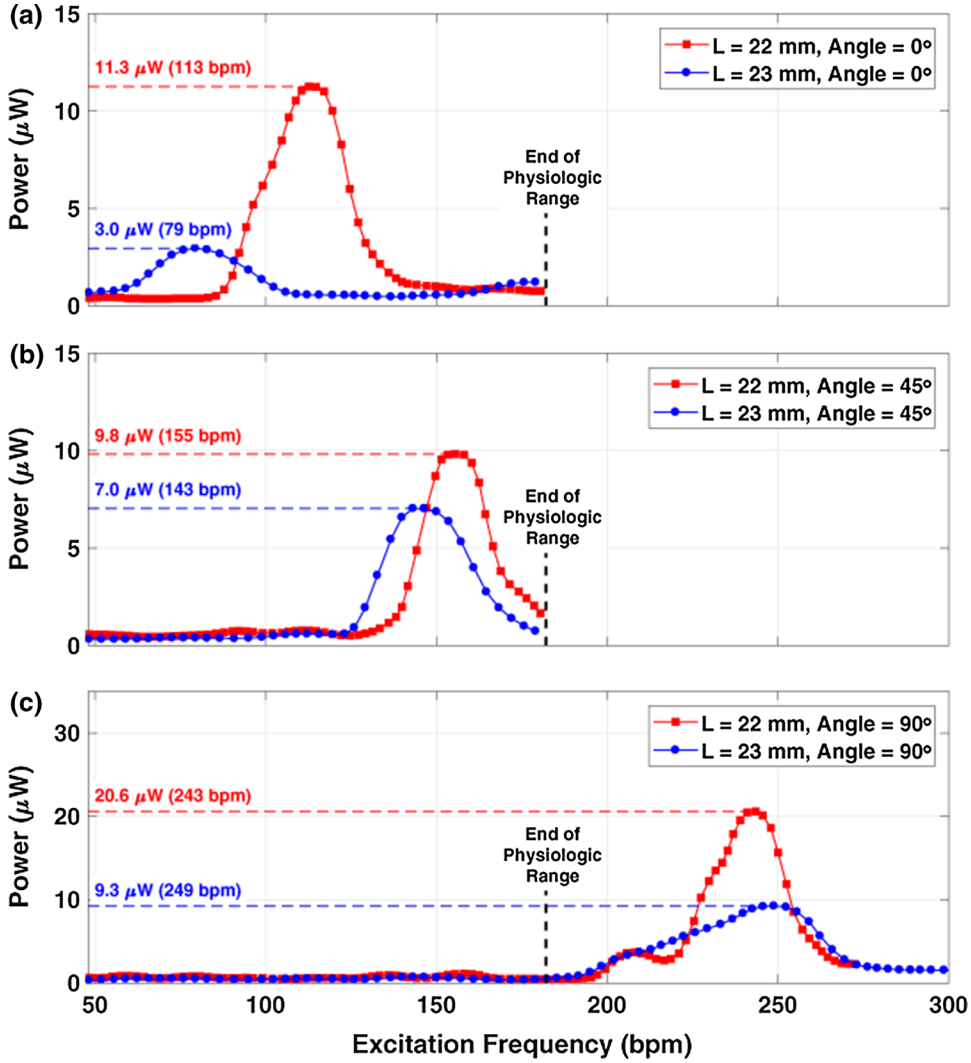

FIGURE 10. Power output as a function of sinusoidal excitation frequency for a 1 mm cantilever length adjustment at three different angle configurations: (a) 0°, (b) 45°, (c) 90°. All plots reflect a 4 mm peak-to-peak axial displacement input.

mm peak-to-peak sinusoid as the dynamic excitation when making power measurements.

The lowest resonant frequencies occur when the device is gravitationally aligned. Figure 10a shows the data obtained when the device is oriented at 0° with respect to gravity as shown in Fig. 9a. In this orientation, the prototype device produces 3.0 μW of power when operating at its lowest resonant frequency of 79 bpm (1.3 Hz). This resonant frequency exceeded the theoretical resonant frequency of 30 bpm, but remains near the lower end of the physiologic range of heart rates. Although the prototype shows a minimum resonant frequency of 79 bpm, it can maintain power output above 1 μW down to 60 bpm. The device can also readily produce higher power at higher excitation frequencies when the cantilever length is reduced. For example, the 1 mm length reduction allowed the device to produce 11.3 μW when operating at the new resonance of 113 bpm (1.9 Hz).

Resonant frequency increases when the device is rotated with respect to gravity. Figure 10b shows the device performance when it is oriented at a 45° angle with respect to gravity as shown in Fig. 9b. The maximum length condition produces a peak power output of 7.0 μW when operating at its resonant frequency of 143 bpm (2.4 Hz) and 9.8 μW following a 1 mm length reduction that shifts the resonant frequency to 155 bpm. Figure 10c shows the device performance when it is oriented at a 90° angle with respect to gravity as shown in Fig. 9c. The maximum length condition produces a peak power output of 9.3 μW when operating at its resonant frequency of 249 bpm (4.2 Hz) and 20.6 μW following a 1 mm length reduction that produces a new resonant frequency at 243 bpm (4.1 Hz).

DISCUSSION

Figure 11 shows the comparison between the experimental and the theoretical resonant frequency predictions. The upper solid line and lower dashed lines represent the predicted resonant frequencies as a function of length for the gravitationally orthogonal and gravitationally aligned cases, respectively. For these calculations, we used the physical parameters listed in "Prototype Description" section. Within the model, the dominant uncertainty arises from the flexural rigidity. Therefore, the plot also shows the bands of resonant frequency curves represented by ± 10% variation in the *EI* model parameter. These bands reveal that the gravitationally aligned resonant frequency prediction is the most sensitive to variations in this parameter. For example, if the flexural rigidity is reduced by 10% from its nominal value, the model predicts a zero resonant frequency (i.e., a transition to the droop failure mode) near 22.1 mm. Because there was no failure mode at this length, our data suggest that the actual prototype is operating with a nominal or above-nominal flexural rigidity. The data points shown in Fig. 11 represent the resonant frequencies shown in Fig. 10, and include error bars for the estimated ± 0.2 mm cantilever length measurement uncertainty. The theoretical and experimental results, when accounting for the attendant uncertainties, show reasonable agreement as discussed below.

The data illustrate the same trends that are predicted theoretically. For a fixed angular orientation, a reduced cantilever length produces an increase in resonant frequency. The exception in our data comes from the gravitationally orthogonal case (Fig. 10c) wherein the resonant power curves show significant overlap. In this case, the resonant frequency of the maximum length condition slightly exceeded the measured resonant frequency of the reduced length condition. This is not a severe theoretical contradiction and is likely attributable to the small inherent resonance sensitivity, the broad, flat peak of the experimental power curves, and length adjustment repeatability in the manual mechanism.

The theoretical analysis also predicts that the resonant frequency for cantilever motion increases as the device transitions from a gravitationally aligned condition to a gravitationally orthogonal condition. This trend is shown unambiguously in the progression between 0° in Fig. 10a to the 90° case in Fig. 10c where the resonant frequencies shift higher in each case. Figure 11 also clearly shows this trend. Additionally, the theoretical analysis predicts a reduction in sensitivity to length adjustments when transitioning from the gravitationally aligned (0°) orientation to the gravitationally orthogonal (90°) orientation. This reduced sensitivity is manifested experimentally given the nearly identical resonant frequencies measured in the gravitationally orthogonal configuration and the highest sensitivity measured in the gravitationally aligned configuration. We conclude that there is significant value in the theoretical model given its ability to guide the construction of a prototype and predict the key trends in the resonant frequency shifts arising from both angular orientation and length adjustment.

Our experimental results also illustrate the viability of the tunable resonance concept for powering implantable medical devices such as a leadless pacemaker. The device power output at conditions of resonance ranged between 3 and 11.3 μW inside of the

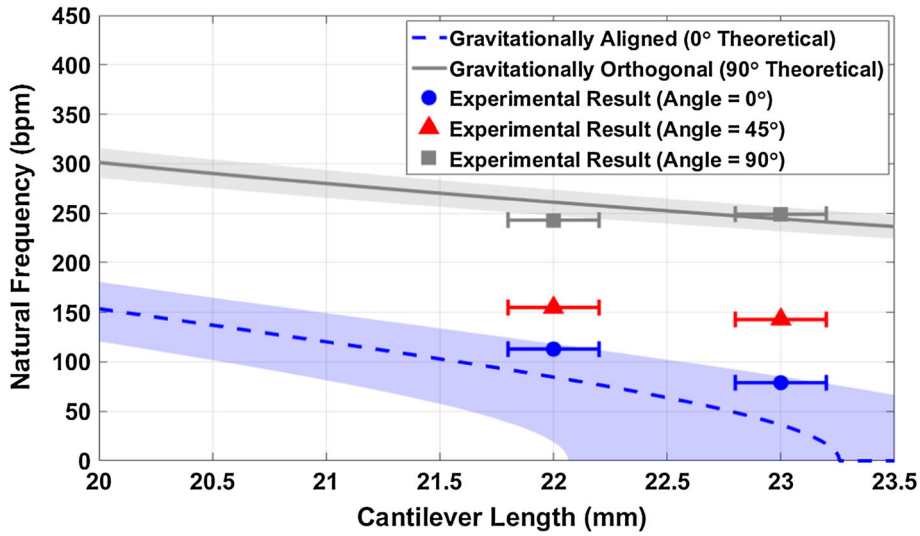

FIGURE 11. Comparison of experimental and theoretical results including theoretical uncertainty bands resulting from ±10% variation in beam flexural rigidity (*EI*) and a constant value of *M* = 0.75.

physiologic range. In conditions of gravitational orthogonality, the peak power became 20.6 μW, although the frequency of excitation must be hyperphysiologic (243 bpm) to achieve this output in the present prototype. The output power values significantly exceed the requirements of a typical leadless pacemaker. For example, a typical leadless pacemaker would require approximately 0.9 μJ to deliver one beat of pacing therapy.[20] At a heart rate of 70 bpm, powering the Micra transcatheter pacemaker system (Medtronic) then requires an average of 1 μW. Additional data suggest that 1 μW may be an overestimate for the Micra system.[19] When therapy delivery features (e.g. pacing) are removed from such devices, the power requirements for simple sensing functionality can also be significantly less than the 1 μW benchmark. For example, 8-bit analog-to-digital CMOS converters have been constructed with power as low as 27 nW.[8] Because our prototype exceeds the 1 μW threshold by more than a factor of three in all of the tested conditions, we conclude that the current prototype will achieve the requisite power for the latest implantable cardiac therapeutic and monitoring devices.

The theoretical model and data also suggest that the implant orientation should be selected such that the device remains in gravitational alignment as much as possible during periods of low activity and low heart rate (e.g., sleep) and maintain a shallow, yet necessarily tilted, angle with respect to gravity during periods of greater activity (e.g., locomotion during the day) when the heart rate is elevated. This strategy would allow the natural variation in gravitational orientation of the patient to coincide with a favorable shift in resonant frequency in the device. Any additional adjustment within the physiologic range would then be achieved through powered cantilever length adjustment.

The collection of power data with our device directly confirms the viability of heart rate sensing using the frequency content of the coil voltage. When the device is used in the high impedance heart rate sensing configuration (see Fig. 2), the signal to noise ratio is also maximized at the given heart rate if the device is in resonance. Sensing the heart rate in this way forms the basis for the device adaptation and length adjustment feedback.

The volume formed by the inner surface of the prototype's enclosure geometry (i.e., subtracting the large wall thickness required for 3D printing fabrication) is approximately 3.3 cm^3. In the context of right ventricular volume, this prototype scale comprises between 2 and 6% of the blood volume in end diastole and end systole, respectively.[16] Given the surplus of power at our modest excitation displacements, our prototype shows promise for further size reduction while continuing to meet the 1 μW threshold.

With a total mass of approximately 7 g, the prototype mass is on the same order as the leadless pacemaker benchmark device,[19,20] whose entire mass (2 g) moves with the apex of the right ventricle during the cardiac cycle. As described in Ref. 31, heart function may not be adversely affected by small harvesting devices given that deposits of surplus epicardial fat can exceed the mass of our device.[26] Therefore, our device is not expected to impart undue metabolic demand on the heart.

Our device relies upon tunable resonance as an essential feature. By adjoining the maxima of the various power curves at different resonant frequencies, the device performance characteristics are significantly enhanced over the case of operating within only one of the power curves. Operating within a single power curve is a constraint of any fixed resonance device. In our case, if we had selected a fixed cantilever length of 22 mm for the device, then the gravitationally aligned device (Fig. 10a) would not be operating optimally unless it were in the narrow neighborhood of heart rates near 113 bpm coincident with the resonance. Furthermore, it would not exceed the 1 μW threshold if the heart rate fell below 89 bpm or exceeded 150 bpm unless the displacement amplitude were increased above our test condition. The tunability of resonant frequency through length adjustment overcomes this limitation, yet use of this feature must be done is such a way as to provide a net positive power budget as discussed in "Design Architecture and Power Budget" section.

CONCLUSIONS

This paper describes a device that utilizes a single magneto-electro-mechanical mechanism intended for both sensing heart rate and adaptively maximizing energy harvesting output through resonant frequency adjustment to match the heart rate. The harvested mechanical energy can then be deployed for myriad purposes including self-sustaining pacing therapy, sensor operation, data logging, or periodic telemetry. A device with the ability to tune resonance to match the heart rate over time endows high signal to noise ratios for heart rate sensing and enhanced energy harvesting output regardless of physiologic state. The design of our device also allows for robustness to external orientation disturbances to the natural frequency by compensating with a commensurate change in length. The need for such compensation, however, is minimized by orienting the implanted device at a suitable angle with respect to gravity.

Our prototype demonstrates resonant frequency tunability across the physiologic range provided that the orientation of the device remains within approximately 45° of the gravitational direction. Estimated power outputs for a 4 mm peak-to-peak displacement were as high as 11.3 μW within the physiologic range of operation. Our conservative displacement test level still shows sufficient power for current benchmark medical devices such as leadless pacemakers. Although the current prototype is larger than a typical leadless pacemaker (e.g., 0.8 cm^3 Ref. 20), epicardial placement may also be a viable alternative even at the scale of our current prototype (3.3 cm^3). Additional design refinement and smaller scale fabrication capabilities will allow us to target the reduced size and catheter deployment shown in Fig. 1.

Our future work is directed toward a fully-integrated, reduced-scale prototype with the attendant sensing and harvesting circuitry. At present, the tunable resonance system performance shows the potential to eliminate the need for batteries in implantable cardiac devices and can provide continuous or near-continuous diagnostic data streams to improve overall patient monitoring and treatment outcomes.

CONFLICT OF INTEREST

Thomas W. Secord is a former employee of Medtronic plc and Milad C. Audi declares that he has no conflict of interest. No benefits in any form have been or will be received from a commercial party related directly or indirectly to the subject of this manuscript.

ETHICAL APPROVAL

This article does not contain any studies with human participants or animals performed by any of the authors.

REFERENCES

[1]Camm, A. J., M. Malik, J. Bigger, G. Breithardt, S. Cerutti, R.J. Cohen, P. Coumel, E. L. Fallen, H.L. Kennedy, R. Kleiger, et al. Heart rate variability. standards of measurement, physiological interpretation, and clinical use. Eur. Heart J. 17(3):354–381, 1996.

[2]Challa, V. R., M. Prasad, Y. Shi, and F. Fisher. A vibration energy harvesting device with bidirectional resonance frequency tunability. Smart Mater. Struc. 17(1):15035, 2008.

[3]Deterre, M., B. Boutaud, R. Dalmolin, S. Boisseau, J.J. Chaillout, E. Lefeuvre, and E. Dufour-Gergam. Energy harvesting system for cardiac implant applications. 2011 Symposium on Design, Test, Integration and Packaging of MEMS/MOEMS (DTIP), pp. 387–391, 2011.

[4]Gieras, J. F., J. H. Oh, M. Huzmezan, and H. S. Sane. Electromechanical energy harvesting system. Patent: US8222775, 2012.

[5]Goto, K., T. Nakagawa, O. Nakamura, and S. Kawata. An implantable power supply with an optically rechargeable lithium battery. IEEE Trans. Biomed. Eng. 48(7):830–833, 2001.

[6]Henderson, D. Simple ceramic motor...inspiring smaller products. 10th International Conference on New Actuators, Bremen, Germany, pp. 1–4, 2006.

[7]Hoffmann, D., A. Willmann, T. Hehn, B. Folkmer, and Y. Manoli, Y. A self-adaptive energy harvesting system. Smart Mater. Struc. 25(3):035013, 2016.

[8]Hu, W., Y. T. Liu, T. Nguyen, D. C. Lie, and B. P. Ginsburg, B.P. An 8-bit single-ended ultra-low-power SAR ADC with a novel DAC switching method and a counter-based digital control circuitry. IEEE Trans. Circ. Syst. 60(7):1726–1739, 2013.

[9]Huikuri, H. V., T. H. Mäkikallio, C. K. Peng, A. L. Goldberger, U. Hintze, M. Møller, et al. Fractal correlation properties of RR interval dynamics and mortality in patients with depressed left ventricular function after an acute myocardial infarction. Circulation 101(1):47–53, 2000.

[10]Karami, A. M., D. J. Inman. Powering pacemakers from heartbeat vibrations using linear and nonlinear energy harvesters. Appl. Phys. Lett. 100(4):042901, 2012.

[11]Khaligh, A., P. Zeng, C. Zheng. Kinetic energy harvesting using piezoelectric and electromagnetic technologies–state of the art. IEEE Trans. Ind. Electron. 57(3):850–860, 2010.

[12]Kluger, J. M., T. P. Sapsis, and A. H. Slocum. Robust energy harvesting from walking vibrations by means of nonlinear cantilever beams. J. Sound Vib. 341:174–194, 2015.

[13]Lee, H. Stability of a cantilever beam with tip mass subject to axial sinusoidal excitations. J. Sound Vib. 183(1):91–98, 1995.

[14]Leland, E. S., and P. K. Wright. Resonance tuning of piezoelectric vibration energy scavenging generators using compressive axial preload. Smart Mater. Struc. 15(5):1413, 2006.

[15]Liu, T., and C. Livemore. Passively tuning harvesting beam length to achieve very high harvesting bandwidth in rotating applications. Proceedings of PowerMEMS pp. 492–495, 2012.

[16]Maceira, A. M., S. K. Prasad, M. Khan, and D. J. Pennell: Reference right ventricular systolic and diastolic function normalized to age, gender and body surface area from steady-state free precession cardiovascular magnetic resonance. Eur. Heart J. 27(23):2879–2888, 2006.

[17]Mah, P.Y. Faraday flashlight. Patent: US6729744, 2004.

[18]Pfenniger, A., M. Jonsson, A. Zurbuchen, V. M. Koch, and R. Vogel. Energy harvesting from the cardiovascular system, or how to get a little help from yourself. Ann. Biomed. Eng. 41(11):2248–2263, 2013.

[19]Reynolds, D., G. Z. Duray, R. Omar, K. Soejima, P. Neuzil, S. Zhang, C. Narasimhan, C. Steinwender, J. Brugada, M. Lloyd, et al. A leadless intracardiac transcatheter pacing system. N. Engl. J. Med. 374(6):533–541, 2016.

[20]Ritter, P., G. Z. Duray, S. Zhang, C. Narasimhan, K. Soejima, R. Omar, V. Laager, K. Stromberg, E. Williams,

and D. Reynolds. The rationale and design of the Micra transcatheter pacing study: safety and efficacy of a novel miniaturized pacemaker. EP Europace 17(5):807–813, 2015.
[21]Romero, E., R. Warrington, M. Neuman. Energy scavenging sources for biomedical sensors. Physiol. Meas. 30(9):R35, 2009.
[22]Secord, T. W., and H. H. Asada. A variable stiffness PZT actuator having tunable resonant frequencies. IEEE Trans. Robot. 26(6):993–1005, 2010.
[23]Secord, T. W., A. J. Johnson. A tunable-resonance faraday device for dual cardiac sensing and energy harvesting. In: IEEE International Symposium on Medical Measurements and Applications (MeMeA), pp. 257–262, 2017.
[24]Sodano, H. A., D. J. Inman, and G. Park. A review of power harvesting from vibration using piezoelectric materials. Shock Vib. Digest 36(3):197–206, 2004.
[25]Tashiro, R., N. Kabei, K. Katayama, E. Tsuboi, and K. Tsuchiya. Development of an electrostatic generator for a cardiac pacemaker that harnesses the ventricular wall motion. J. Artif. Organs 5(4):0239–0245, 2002.
[26]Thanassoulis, G., J. M. Massaro, U. Hoffmann, A. Mahabadi, R. S. Vasan, C. J. O'Donnell, and C. S. Fox. Prevalence, distribution, and risk factor correlates of high pericardial and intrathoracic fat depots in the framingham heart study. Circulation: Cardiovasc. Imaging 3(5):559–566, 2010.
[27]Von Büren, T., and G. Tröster. Design and optimization of a linear vibration-driven electromagnetic micro-power generator. Sens. Actuat. A: Phys. 135(2):765–775, 2007.
[28]Wu, W. J., Y. Y. Chen, B. S. Lee, J. J. He, and Y.T. Peng. Tunable resonant frequency power harvesting devices. In: Smart Structures and Materials, p. 61690A. International Society for Optics and Photonics, 2006.
[29]Wu, X., J. Lin, S. Kato, K. Zhang, T. Ren, and L. Liu. A frequency adjustable vibration energy harvester. Proceedings of PowerMEMS, pp. 245–248, 2008.
[30]Zurbuchen, A., A. Haeberlin, L. Bereuter, A. Pfenniger, S. Bosshard, M. Kernen, P. P. Heinisch, J. Fuhrer, and R. Vogel. Endocardial energy harvesting by electromagnetic induction. IEEE Trans. Biomed. Eng. 65(2):424–430, 2018.
[31]Zurbuchen, A., A. Pfenniger, A. Stahel, C. T. Stoeck, S. Vandenberghe, V. M. Koch, and R. Vogel. Energy harvesting from the beating heart by a mass imbalance oscillation generator. Ann. Biomed. Eng. 41(1):131–141, 2013.